Photonic-Assisted Microwave Temporal Convolution

Jiejun Zhang, *Student Member, IEEE*, and Jianping Yao, *Fellow, IEEE, Fellow, OSA*

***Abstract*—An approach to performing photonic-assisted temporal convolution of two microwave signals is proposed and experimentally demonstrated. Temporal convolution involves three operations: time reversal of one microwave signal, the multiplication of the time-reversed signal with a second microwave signal, and the integration of the multiplied microwave signal, which can be implemented optically by a linearly chirped fiber Bragg grating (LCFBG), a Mach-Zehnder modulator, and a second LCFBG in conjunction with a low-speed photodetector, respectively. The proposed temporal convolution is experimentally evaluated, in which the calculation of three temporal convolutions between two rectangular waveforms, between an inverse sawtooth waveform and a rectangular waveform, and between an arbitrary waveform and a short pulse is experimentally demonstrated.**

***Index Terms*—Convolution, integrator, microwave photonics, optical signal processing, time reversal.**

I. Introduction

PHOTONIC signal processing is considered a solution to overcome the bandwidth bottleneck of conventional electronic signal processors, which is caused by the limited sampling speed of electronic circuits [1], [2]. So far, most of the important signal processing functions can be performed using photonic techniques, such as Fourier transform [3], Hilbert transform [4], microwave filtering [5], complex conjugation [6]–[9], temporal integration [10]–[17] and differentiation [18], and correlation [19]. However, temporal convolution between two microwave signals, also a very important signal processing function, has not yet been proposed and demonstrated using photonic techniques.

The convolution of two microwave signals, here we call it temporal convolution, is different from a filtering operation where a microwave signal is convolved with the impulse response of a microwave filter due to the multiplication between the spectrum of the microwave input signal and the frequency response of the microwave filter. In many cases, temporal convolution can provide better flexibility in signal processing as compared with a filtering operation since the spectral response of a filter is fixed and may not be tunable easily at a high speed. For many signal processing applications, however, the spectra of the two microwave signals to be convolved need to be performed with one of the two signals or both signals being updated in real time. For example, the temporal convolution has been used for real-time distortion correction in an imaging processing system [20] where image deblur could be achieved by convolving the image signal with an impulse response function measured for the specific distortion. In [21], the detection of the phase information of a periodic signal imbedded in a noise was realized by convolving the corrupted signal with its cumulant (accumulation with certain algorithm) version. The convolution operations reported in [20] and [21] were done based on digital signal processing. The convolution of two signals using an analog system, especially a photonic analog system, has a high potential to achieve a much faster operation speed and a larger bandwidth.

Temporal convolution between two signals f and g is expressed as

$$f * g = \int_{-\infty}^{\infty} f(\tau)\, g(t-\tau)\, d\tau \tag{1}$$

where the symbol $*$ represents convolution operation. According to (1), the calculation of temporal convolution involves three operations,

1) Time reversal of one of the input signal, $g(\tau)$ for instance, to get $g(-\tau)$;
2) Multiplication between $f(\tau)$ and a time-delayed $g(t-\tau)$;
3) Integration of the multiplication result, which gives the convolution result for a given time delay t.

To get a final convolution result, operations 2) to 3) should be repeated with an incremental time delay t. It can be seen that temporal convolution is more complicated to implement than the other signal processing functions, as reported in [3]–[19]. However, thanks to the progress in photonic signal processing techniques in the past few years, the operations stated above can be performed using photonic techniques.

Specifically, microwave time reversal can be implemented using photonic techniques. Photonic microwave time reversal was first demonstrated based on the three photon echo effect [6], [7], in which an extremely long reversal time window of 6 μs was achieved. However, the operation bandwidth is small, which is limited to 10 MHz. Recently, we demonstrated a technique to implement temporal reversal using a single linearly chirped fiber Bragg grating (LCFBG), in which a precise time reversal with an operation bandwidth as wide as 4 GHz within a reversal time window of 10 ns was achieved [8], [9]. The microwave time reversal solutions reported in [6]–[9] can be used for implementing temporal convolution.

The multiplication of two microwave signals can also be achieved using photonic techniques. For example, we can use an electro-optic modulator to perform the multiplication of two microwave signals.

Photonic integration of an optical or microwave signal can be achieved using photonic techniques. Numerous approaches have been reported, which can be realized using a fiber Bragg grating

Manuscript received January 17, 2016; revised June 13, 2016 and August 17, 2016; accepted August 23, 2016. Date of publication August 24, 2016; date of current version September 25, 2016. This work was supported by the Natural Sciences and Engineering Research Council (NSERC) of Canada. The work of J. Zhang was supported by the China Scholarship Council.

The authors are with the Microwave Photonics Research Laboratory, School of Electrical Engineering and Computer Science, University of Ottawa, Ottawa, ON K1N 6N5, Canada (e-mail: jpyao@eecs.uottawa.ca).

Color versions of one or more of the figures in this paper are available online at http://ieeexplore.ieee.org.

Digital Object Identifier 10.1109/JLT.2016.2603067

0733-8724 © 2016 IEEE. Personal use is permitted, but republication/redistribution requires IEEE permission.
See http://www.ieee.org/publications_standards/publications/rights/index.html for more information.

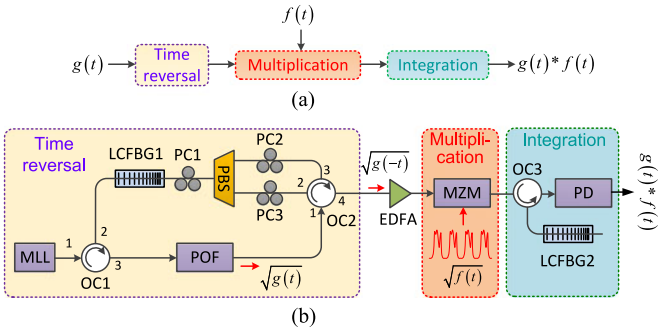

Fig. 1. (a) Temporal convolution of two microwave signals. (b) Schematic diagram of the proposed temporal convolution system. MLL: mode-locked laser; OC: optical circulator; POF: programmable optical filter; LCFBG: linearly chirped fiber Bragg grating; PC: polarization controller; PBS: polarization beam splitter; EDFA: erbium-doped fiber amplifier; MZM: Mach-Zehnder modulator; PD: photodetector.

(FBG) [10], a microring resonator [11], [12], an active Fabry-Perot cavity [13], or an optical dispersive device [14]–[17].

Although the implementation of the three operations involved in temporal convolution has been proposed, the key challenge in realizing temporal convolution is to realize a variable time delay difference between the two microwave signals. In this paper, we propose and experimentally demonstrate a photonic approach to performing temporal convolution between two microwave signals in which the three operations of time reversal, multiplication and integration are implemented based on an LCFBG (the first LCFBG), a Mach-Zehnder modulator (MZM), and a second LCFBG in conjunction with a photodetector (PD), respectively. The variable time delay of one of the microwave signals is achieved by generating two sequences of replicas of the two microwave signals with slightly different repetition rates. The two sequences are multiplied at the MZM and integrated by the second LCFBG. The convolution result is obtained at the output of a PD. Since the PD here is used to detect the signal energy, a small bandwidth of the PD will be sufficient to perform the proposed temporal convolution in which the two microwave signals can be wideband. The proposed approach is experimentally evaluated, in which the calculations of three temporal convolutions between two rectangular waveforms, between an inverse sawtooth waveform and a rectangular waveform, and between an arbitrary waveform and a short pulse are experimentally demonstrated.

II. Principle

Fig. 1(a) shows the temporal convolution of two microwave signals denoted as $f(t)$ and $g(t)$, which involves three operations, microwave time reversal, multiplication and integration. The three operations can be performed using three subsystems in the optical domain. Fig. 1(b) shows the implementation of temporal convolution of two microwave signals in the optical domain. The first subsystem is used for achieving time reversal, which is similar to the approach we introduced in [9], where a mode-locked laser (MLL) is employed to generate a transform-limited pulse train. An optical pulse in the pulse train is first reflected by an LCFBG (LCFBG1) through an optical circulator (OC1), and then spectrally shaped by a programmable optical filter (POF), to encode a microwave waveform to make the spectral response of the POF have a shape that is identical to the microwave waveform. The second subsystem is for achieving multiplication, which is implemented by simply using an MZM, to which a second microwave signal is applied via its electrical port. The integration is performed by a third subsystem that consists of a second LCFBG (LCFBG2) and a low-speed PD. Since the input signals are faster than the response time of the PD, the output of the PD is in fact proportional to the optical energy that it receives within its response time window, i.e., the integration of the power of the fast input signal. To get the integration for the amplitude of the signals as indicated in (1), the input signals $f(t)$ and $g(t)$ should be preprocessed to have only positive values, and then converted to $\sqrt{f(t)}$ and $\sqrt{g(t)}$. Note that if the integration is performed in the optical domain (without photo-detection), the preprocessing is not needed. In the following, for simplicity, assume we have two input signals given by $\sqrt{f(t)}$ and $\sqrt{g(t)}$.

For a microwave signal $\sqrt{g(t)}$, the POF can be configured to have a spectral response that has an identical shape as the microwave signal, $\sqrt{g(\omega)}$, where ω is the optical angular frequency given by $\omega = t/\ddot{\Phi}$ and $\ddot{\Phi}$ (in ps^2) is the dispersion coefficient of LCFBG1 when looking into it from the left end [22]. The spectrum is linearly mapped to the time domain through wavelength-to-time mapping at LCFBG1 from the left end [22]. After reflected by LCFBG1 the second time from its right side, wavelength-to-time mapping is performed and a time-reversed microwave signal $\sqrt{g(-t)}$ is obtained [9]. Note that the dispersion coefficient of LCFBG1 when looking into it from the right end is $-\ddot{\Phi}$. $\sqrt{g(t)}$ can also be encoded to a pulse in the pulse train with the temporal pulse shaping approach [22], where an MZM is used instead of the POF, but the microwave signal applied to the MZM must be synchronized to the pulse in the pulse train. The two techniques are equivalent. Here we choose the wavelength-to-time mapping approach using a POF as it does not require any synchronization between the waveform from the MLL and the waveform from an arbitrary waveform generator (AWG), thus it is simpler experimentally. Three polarization controllers (PCs) are used to ensure that the pulse can be reflected by LCFBG1 via the right end twice and to achieve a maximum coupling efficiency [9]. Since the spectral response of the POF is not updated on a pulse-by-pulse basis [23], $\sqrt{g(-t)}$ is repeating at a repetition rate identical to that of the pulse train from the MLL. An erbium-doped fiber amplifier (EDFA) is used after the time reversal subsystem to compensate for the losses of the POF, the PBS, and LCFBG1. Note that although $\sqrt{g(-t)}$ can be generated by letting an MLL pulse reflected only once from the right end of LCFBG1 after being filtered by the POF with a modified spectral response to encode $\sqrt{g(-t)}$, in the proposed approach we use LCFBG1 three times to encode $\sqrt{g(t)}$ based on the temporal pulse shaping approach. An added advantage is that an MZM can be employed to replace the POF to provide better flexibility in signal processing since the signal applied to the MZM can be updated in real time.

The amplified pulses in the pulse train encoded by $\sqrt{g(-t)}$ are then sent to the multiplication subsystem, which is simply the MZM. The second microwave signal to be convolved, $\sqrt{f(t)}$,

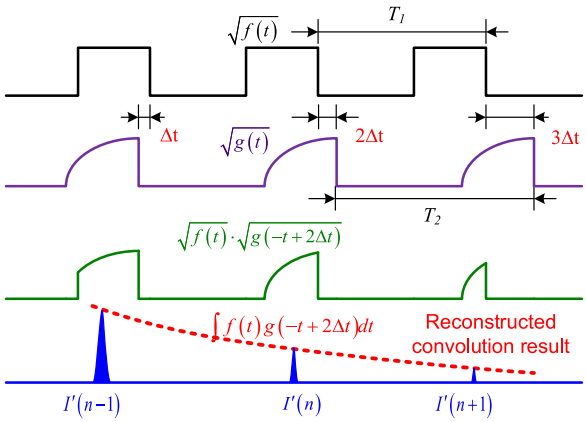

Fig. 2. Operation principle of the proposed temporal convolution system. An rectangular waveform *f*(*t*) and a sawtooth waveform *g*(*t*) are used as the two signals to be convolved.

is generated by the AWG with a repetition rate slightly different from that of the pulse train from the MLL, and is applied to the MZM. The multiplied signal at the output of the MZM is then launched into LCFBG2 for integration. LCFBG2 has a dispersion coefficient that is identical to that of LCFBG1 when looking into it from the left end. The signal at the output of LCFBG2 is converted to the electrical domain at the PD. Integration will be performed at the same time thanks to the small bandwidth of the PD.

To illustrate the operation of the system, the convolution between a rectangular waveform *f*(*t*) and an inverse sawtooth waveform *g*(*t*) is used as an example, as shown in Fig. 2. First, $\sqrt{f(t)}$ and $\sqrt{g(-t)}$ are generated with two slightly different repetition periods of T_1 and T_2, respectively. There is a slight difference of Δt between T_1 and T_2. Due to the difference between the repetition periods of the two signals, a changing time delay difference can be achieved between the replicas of $\sqrt{f(t)}$ and $\sqrt{g(-t)}$ after a different number of periods *n*. The two signals are then multiplied and integrated. The output of the integration subsystem is a series of short pulses with different peak powers. The convolution result *I'*(*n*) can be reconstructed from the amplitudes of the peaks. Note that *I'*(*n*) is the integration of the *n*-th pulse in the pulse train. Therefore, it is discrete, and the corresponding unit time increase along the horizontal axis is $|T_1 - T_2|$ for the convolution result.

Mathematically, a time reversed signal on an optical pulse at the output of the time reversal subsystem (port 4 of OC2) can be expressed as [9],

$$r_i(t) = \exp\left(\frac{jt^2}{2\ddot{\Phi}}\right)\sqrt{g(-t)} \tag{2}$$

where $\sqrt{g(t)}$ is seen as the pre-processed input microwave signal. It should be noted that $\sqrt{g(t)}$ is encoded by the POF, to simplify the experimental implementation. For real applications, the microwave signal can be modulated on an optical pulse at an optical modulator, and thus the POF is no longer needed. According to [22], an optical pulse modulated by $\sqrt{g(t)}$ can have an identical expressed as (2). The quadratic phase term in (2) is induced by LCFBG1 and used for the time reversal [8]. This phase term will be eliminated at the PD after photo-detection. Considering that the time-reversed microwave signal is carried by the optical pulse train, we have

$$r(t) = r_i(t) * \sum_{n=0}^{N-1}\delta(t - nT_1) = \sum_{n=0}^{N-1} r_i(t - nT_1) \tag{3}$$

where δ is the Dirac delta function, T_1 is the period of the pulse train from the MLL, *n* is an integer and $N = 1/|T_1 - T_2|$. Similarly, the other pre-processed microwave signal, $\sqrt{f(t)}$, is repeating at a slightly different repetition rate with a period of T_2. The signal applied to the MZM is expressed as

$$s(t) = \sum_{n=0}^{N-1}\sqrt{f(t - nT_2)} \tag{4}$$

The two signals *r*(*t*) and *s*(*t*) are then multiplied at the MZM. The time intervals T_1 and T_2 are chosen to be much larger than the temporal duration of the input waveforms to avoid overlapping between any two adjacent waveforms, and the difference between T_1 and T_2 is chosen to be small, so that we only need to consider the terms with the same value of *n* in (3) and (4) to overlap in time within the summation range of *N*-1, i.e., the multiplication will only take place for the terms with the same value of *n*. At the output of the MZM, the signal can be expressed as

$$m_n(t) = r_i(t - nT_1) \times \sqrt{f(t - nT_2)} \tag{5}$$

The time delay difference between $r_n(t)$ and $\sqrt{f(t - nT_2)}$ is $n \times (T_2 - T_1)$. As *n* changes, a different time delay difference between the two waveforms is resulted, which is required by the temporal convolution.

The multiplication output is then directed to LCFBG2 for the first step of the integration operation. After propagating through LCFBG2 with a dispersion coefficient of $\ddot{\Phi}$, which is identical to that of LCFBG1 when looking into it from the left end, we obtain the output signal as a convolution between $m_n(t)$ and the impulse response of LCFBG2, given by

$$y(t) = m_n(t) * \exp\left(-\frac{jt^2}{2\ddot{\Phi}}\right) \tag{6}$$

By using the wavelength-to-time mapping relationship [22], we get

$$y(t) = \exp\left(-\frac{jt^2}{2\ddot{\Phi}}\right) \times F[m_n(t)] \tag{7}$$

where *F* denotes Fourier transform. The signal is then detected at the PD, which is the second step of the integration operation, generating an output current given by

$$\begin{aligned} I(t) &= \Re|y(t)|^2 \\ &= \Re\left|\exp\left(-\frac{jt^2}{2\ddot{\Phi}}\right) \times F[m_n(t)]\right|^2\Big|_{\omega=-\frac{t}{\ddot{\Phi}}} \\ &= \Re|F[m_n(t)]|^2\Big|_{\omega=-\frac{t}{\ddot{\Phi}}} \end{aligned} \tag{8}$$

where $\Re$ is the responsivity of the PD. It can be seen that the signal at the output of the PD is actually the power spectrum of the multiplication result in (5), rather than its integration. However, it should be noted if the bandwidths of the input signals are small compared to the optical carrier frequency, $I(t)$ becomes a very short optical pulse with a pulse width given by $\delta t = \delta\omega \cdot \ddot{\Phi}$, where $\delta\omega$ is the electrical bandwidth of the multiplication result in (5). If δt is smaller than the response time of the PD, the output current will be proportional to the energy of a pulse, which is the integration of the pulse spectrum, thus we have

$$I'(n) = \Re \int_{\delta\tau} |y(t)|^2 dt = \Re \int_{\delta\omega} |F[m_n(t)]|^2 d\omega \quad (9)$$

According to the Parseval's theorem, for each pulse, we have the output given by

$$I'(n) = \Re \times \frac{1}{2\pi} \int_{\delta t} |m_n(t)|^2 dt \quad (10)$$

Substitute (2) and (5) into (10), we get

$$I'(n) = \Re \times \frac{1}{2\pi} \int_{\delta t} g(-t + nT_1) f(t - nT_2) dt \quad (11)$$

Compare (11) with (1), $I'(n)$ can be seen as the convolution between signals $g(t)$ and $f(t)$, with a time delay difference of $n \times (T_2 - T_1)$. For a different n, the convolution result provides a value corresponding to a different time delay difference.

Note that the convolution process described above requires that the two signals are periodic. For one of the signal that is not periodic, the system can also be used to perform convolution, but a fiber-optic recirculating loop [24] should be used to convert the aperiodic signal into a periodic signal in which the repetition rate of the converted signal can be controlled by choosing the length of the fiber-optic recirculating loop.

In the proposed system, the PD is used to measure the energies rather than the temporal shapes of the pulses, thus the required bandwidth can be much smaller than the bandwidths of the input signals. In fact, it is only required that the response time of the PD is shorter than T_1 and T_2. Note that integration is possible even without the use of LCFBG2, but the response time of the PD should be notably longer than the duration of the pulse that arrive at the PD. In this case, however, the response time window for the PD is small which makes it difficult to find a PD to meet the requirement. When LCFBG2 is used, the duration of the pulse arriving at the PD is significantly reduced, making it much easier to find a PD to meet the requirement. In addition, the system is more adaptable for an input signal with a different repetition period and pulse duration when LCFBG2 is used.

The preprocessing that converts the input signals to their square roots is required since the final step of integration is realized by the small-bandwidth PD, and the signal at the output of the PD, which is in the electrical domain, is proportional to the power of the input optical signal. If an all-optical integrator is implemented instead, the preprocessing will not be needed.

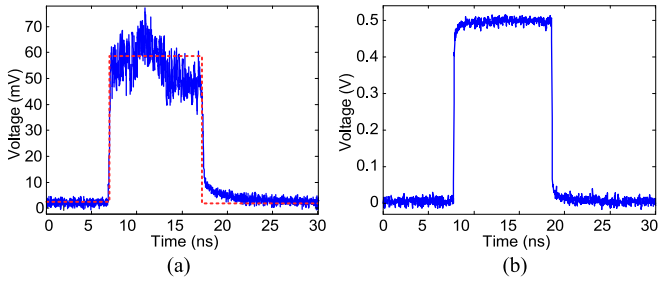

Fig. 3. Two rectangular waveforms used as the input waveforms for temporal convolution. (a) Square root of $g(t)$ encoded by the POF. Blue line: the measured waveform at the output of the POF; red dotted line: an ideal rectangular waveform. (b) Square root of $f(t)$ generated by the AWG.

III. Experiment

An experiment based on the system shown in Fig. 1 is performed. A wavelength tunable MLL (PriTel FFL-1550-20) is used as the optical source, which generates an optical pulse train with a repetition rate of 20 MHz or a period of 50 ns. The 3-dB spectral width and temporal width of a pulse in the pulse train is 8 nm and 600 fs, respectively. LCFBG1 and LCFBG2 are fabricated to have an identical bandwidth of 4 nm and a dispersion coefficient of $\pm$2500 ps/nm. A POF (Finisar WaveShaper 4000 s) is used to encode one of the input signal to the MLL pulses. The other input signal is generated by an AWG (Tektronix AWG7102) with a sampling rate of 10 Gb/s and applied to an 10-GHz MZM (JDS-U OC-192) to perform signal multiplication. The AWG is configured to generate a waveform with a period 1% longer than that of the pulse train from the MLL, i.e., 50.5 ns. The convolution result at the output of the PD (New Focus 1414, 25 GHz) is sampled by a real-time oscilloscope (Agilent 93204A).

The POF has a spectral resolution of 10 GHz, which can generate $\sqrt{g(t)}$ at an equivalent sampling rate of 5 Gb/s when working in conjunction with LCFBG1. Hence, both $f(t)$ and $g(t)$ have an analog bandwidth of less than 5 GHz [22]. According to (8), the pulse width is around 200 ps after integration, which is larger than the response time of the PD and that of the oscilloscope. To satisfy the condition given in (9), a digital low-pass filter with a cutoff frequency at 1 GHz is adopted for the signal sampled by the oscilloscope. In fact, it is only required that the PD has a response time faster than the period of the waveforms to be convolved, which is 50 ns in our experiment. Although the system performs convolution for two signals with relatively large bandwidths, only a low-speed PD and a low-speed sampling system are required to acquire the convolution result, which can be a great advantage for the proposed system. It should be noted that, each MLL pulse is temporally stretched to have a duration of 10 ns by LCFBG1, indicating that the system can only process an input signal with a temporal duration less than 10 ns.

Then, we use different waveform pairs to test the operation of the proposed temporal convolution system. The waveform pairs include two rectangular waveforms, a rectangular waveform and an inverse sawtooth waveform, and an arbitrary waveform and a short pulse. Fig. 3 shows the two rectangular waveforms with

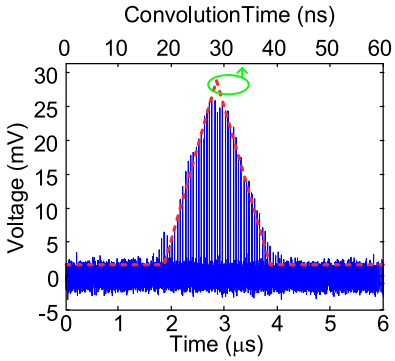

Fig. 4. The convolution between two rectangular waveforms. Red-dotted line: the theoretical convolution output of the two rectangular waveforms with the upper horizontal axis; blue line: the measured convolution output with the lower horizontal axis, which is a series of pulses with the peak amplitudes representing the convolution result.

temporal widths of 10 ns that are generated by the POF and the AWG, respectively. Although a rectangular $g(\omega)$ is applied to the POF, some ripples can be found in the generated waveform shown in Fig. 3(a) due to the uneven optical spectrum of the MLL pulse and the uneven gain spectrum of the EDFA. The rectangular waveform generated by the AWG is very close to an ideal rectangular waveform. It is known that the convolution of two rectangular waveforms with an identical temporal width is a triangular waveform, and the rise time of the triangular waveform should be equal to the width of one of the input rectangular waveform. Fig. 4 shows the experimentally obtained convolution output (blue line). An ideal convolution result (red-dotted line) is also shown for comparison. The output signal is a series of short pulses, with the peak amplitude profile nicely fits to the ideal convolution. It should be noted that two time scales for the horizontal axes are used in Fig. 4, where the lower horizontal axis represents the time for the measured output and the upper horizontal axis represents the time for the convolution, which is recovered by using $n \times (T_2 - T_1)$ with n from 0 to N-1. As we have discussed, the convolution results are discrete values given by the measured the energies of the pulses. The corresponding time axis should also be discrete, with a unit time increment given by $(T_2 - T_1)$. In our case, $(T_2 - T_1) = 0.01 \times T_1$. The upper horizontal axis corresponding to the convolution is simply obtained by multiplying the real time in the lower horizontal axis by 0.01.

An asymmetric waveform which is an inverse sawtooth waveform is then used to test the temporal convolution system. Again, by configuring the POF to have a spectral response of $\sqrt{g(\omega)}$, where $g(\omega)$ has an inverse sawtooth shape, the square root of an inverse sawtooth waveform with a temporal duration of 10 ns is obtained at the output of the time reversal subsystem, as shown in Fig. 5(a). The waveform is then convolved with the rectangular waveform shown in Fig. 3(b). Fig. 5(b) shows the convolution result. A good agreement between the theoretical and the measured results is achieved. For convolution operation, we know that $f * g = g * f$, i.e., no matter which function is temporally reversed, the convolution result should be the same. In our system, however, the convolution output may be temporally reversed if a different input signal is temporally reversed. But

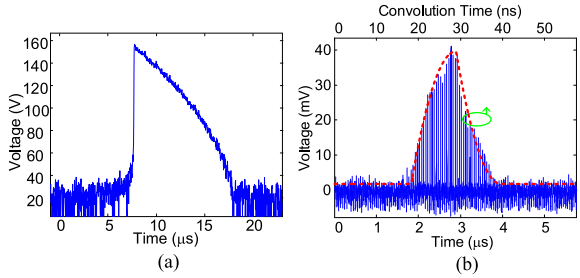

Fig. 5. (a) The square root of an inverse sawtooth waveform achieved at the output of the POF; (b) the convolution between a rectangular waveform and an inverse sawtooth waveform. Red dotted line: the theoretical convolution output of a rectangular waveform with an inverse sawtooth waveform, blue line: the measured convolution output of the system.

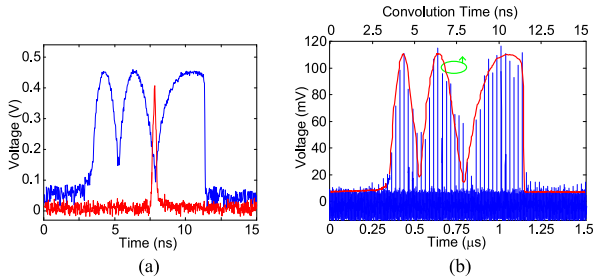

Fig. 6. (a) The square root of a short pulse achieved at the output of the POF (red) and the square root of a three-cycle chirped waveform generated by the AWG (blue); (b) the convolution between a three-cycle chirped waveform and a short pulse. Red line: theoretical convolution result; blue line: the measured output of the convolution system, when the three-cycle chirped waveform is convolved with a short pulse with a temporal width of 400 ps.

the sign of $(T_2 - T_1)$ will also be changed for $f * g$ and $g * f$. The time in the horizontal axis for convolution $n \times (T_2 - T_1)$ will then be reversed, which results in a consistent convolution results for both $f * g$ and $g * f$.

Finally, we investigate the convolution between a complex waveform and a short pulse. The complex waveform is a three-cycle chirped waveform, which is generated by the AWG. The POF is configured to have a narrow passband of 20 GHz which leads to the generation of a short pulse with a temporal width of 400 ps after wavelength-to-time mapping by LCFBG1. The generated square root of the three-cycle chirped waveform and the short pulse are shown in Fig. 6(a). The convolution of a waveform and an ultra-short pulse (ideally a unit impulse function) should be the waveform itself. Fig. 6(b) shows the theoretical convolution result and the measured convolution output of the system. Note that the vertical axis does not represent the actual voltage level of the three-cycle chirped waveform generated by the AWG, which has a peak voltage of 0.5 V (refer to Fig. 3(b)). Again, the measured result is in good agreement with theoretical result. For a complex waveform with more details, to get a more smooth convolution result, one may use a smaller value of $|T_2 - T_1|$, so that the convolution can be calculated with a higher time resolution.

IV. Conclusion

We have proposed and experimentally demonstrated a photonic system that can perform temporal convolution of two microwave waveforms, which was realized by three photonic

subsystems to perform time reversal, signal multiplication, and integration. The key challenge in performing temporal convolution was to realize a variable time delay difference between the two microwave waveforms, which was achieved by generating two sequences of replicas of the two microwave waveforms with two slightly different repetition rates. The two sequences were multiplied at the MZM and integrated by LCFBG2 followed by the photo-detection at the PD, with the convolution result obtained at the output of a PD. Since the PD here is used to detect the pulse energy, a small bandwidth of the PD will be sufficient to perform the proposed temporal convolution in which the two microwave waveforms could be wideband. The proposed approach was experimentally evaluated, in which the calculations of three temporal convolutions between two rectangular waveforms, between an inverse sawtooth waveform and a rectangular waveform, and between an arbitrary waveform and a short pulse were experimentally demonstrated.

REFERENCES

[1] R. Minasian, "Photonic signal processing of microwave signals," *IEEE Trans. Microw. Theory Techn.*, vol. 54, no. 2, pp. 832–846, Feb. 2006.

[2] J. Capmany, J. Mora, I. Gasulla, J. Sancho, J. Lloret, and S. Sales, "Microwave photonic signal processing," *J. Lightw. Technol.*, vol. 31, no. 4, pp. 571–586, Feb. 2013.

[3] M. A. Muriel, J. Azaña, and A. Carballar, "Real-time Fourier transformer based on fiber gratings," *Opt. Lett.*, vol. 24, no. 1, pp. 1–3, Jan. 1999.

[4] J. Zhang, W. Liu, F. Kong, and J. P. Yao, "Microwave Hilbert transformer based on a single passband microwave photonic filter for simultaneous channel selection and signal processing," *J. Lightw. Technol.*, vol. 32, no. 17, pp. 2996–3001, Sep. 2014.

[5] J. Capmany, B. Ortega, and D. Pastor, "A tutorial on microwave photonic filters," *J. Lightw. Technol.*, vol. 24, no. 1, pp. 201–229, Jan. 2006.

[6] H. Linget, L. Morvan, J.-L. Le Gouët, and A. Louchet-Chauvet, "Time reversal of optically carried radiofrequency signals in the microsecond range," *Opt. Lett.*, vol. 38, no. 5, pp. 643–645, Mar. 2013.

[7] H. Linget, T. Chanelière, J.-L. Le Gouët, and A. Louchet-Chauvet, "Time reversal of light by linear dispersive filtering near atomic resonance," *New J. Phys.*, vol. 15, Jun. 2013, Art. ID 063037.

[8] J. Zhang and J. P. Yao, "Broadband and precise microwave time reversal using a single linearly chirped fiber Bragg grating," in *Proc. Int. Topical Meeting Microw. Photon. 9th Asia–Pacific Microw. Photon. Conf.*, Oct. 2014, pp. 57–60, paper TuD-2.

[9] J. Zhang and J. P. Yao, "Broadband and precise microwave time reversal using a single linearly chirped fiber Bragg grating," *IEEE Trans. Microw. Theory Techn.*, vol. 63, no. 7, pp. 2166–2172, Jul. 2015.

[10] R. Slavík, Y. Park, N. Ayotte, S. Doucet, T.-J. Ahn, S. LaRochelle, and J. Azaña, "Photonic temporal integrator for all-optical computing," *Opt. Exp.*, vol. 16, no. 22, pp. 18202–18214, Oct. 2008.

[11] W. Liu, M. Li, R. S. Guzzon, E. J. Norberg, J. S. Parker, L. A. Coldren, and J. P. Yao, "Photonic temporal integrator with an ultra-long integration time window based on an InP-InGaAsP integrated ring resonator," *J. Lightw. Technol.*, vol. 32, no. 20, pp. 3654–3659, Oct. 2014.

[12] M. Ferrera, C. Reimer, A. Pasquazi, M. Peccianti, M. Clerici, L. Caspani, S. T. Chu, B. E. Little, R. Morandotti, and D. J. Moss, "On-chip CMOS-compatible all-optical integrator," *Nat. Comm.*, vol. 1, p. 29, Jun. 2010.

[13] N. Huang, M. Li, R. Ashrafi, L. Wang, X. Wang, J. Azaña, and N. Zhu, "Active Fabry-Perot cavity for photonic temporal integrator with ultra-long operation time window," *Opt. Exp.*, vol. 22, no. 3, pp. 3105–3116, Feb. 2014.

[14] Y. Park and J. Azaña, "Ultrafast photonic intensity integrator," *Opt. Lett.*, vol. 34, no. 8, pp. 1156–1158, Apr. 2009.

[15] M. H. Asghari, Y. Park, and J. Azaña, "Photonic temporal integration of broadband intensity waveforms over long operation time windows," *Opt. Lett.*, vol. 36, no. 18, pp. 3557–3559, Sep. 2011.

[16] A. Malacarne, R. Ashrafi, M. Li, S. LaRochelle, J. P. Yao, and J. Azaña, "Single-shot photonic time-intensity integration based on a time-spectrum convolution system," *Opt. Lett.*, vol. 37, no. 8, pp. 1355–1357, Apr. 2012.

[17] H. Jiang, L. Yan, J. Ye, W. Pan, B. Luo, and X. Zou, "Tunable microwave photonic temporal signal processor: Differentiator and integrator," *IEEE Photon. Technol. Lett.*, vol. 25, no. 23, pp. 2358–2361, Dec. 2013.

[18] M. Li, L.-Y. Shao, J. Albert, and J. P. Yao, "Continuously tunable photonic fractional temporal differentiator based on a tilted fiber Bragg grating," *IEEE Photon. Technol. Lett.*, vol. 23, no. 4, pp. 251–253, Feb. 2011.

[19] H. Yu, W. Fang, X. Wu, X. Lin, L. Tong, W. Liu, A. Wang, and Y. R. Shen, "Single nanowire optical correlator," *Nano Lett.*, vol. 14, no. 6, pp. 3487–3490, May 2014.

[20] A. E. Campbell-Washburn, H. Xue, R. J. Lederman, A. Z. Faranesh, and M. S. Hansen, "Real-time distortion correction of spiral and echo planar images using the gradient system impulse response function," *Magn. Resononance Med.*, 10.1002/mrm.25788, Jun. 2015.

[21] M. E. I. Martínez and F. E. H. Montero, "Detection of periodic signals in noise based on higher-order statistics joined to convolution process and spectral analysis," in *Progress in Pattern Recognition, Image Analysis, Computer Vision, and Applications*, New York, NY, USA: Springer, 2013, pp. 488–495.

[22] J. P. Yao, "Photonic generation of microwave arbitrary waveforms," *Opt. Commun.*, vol. 284, no. 15, pp. 3723–3736, Jul. 2011

[23] S. T. Cundiff and A. M. Weiner, "Optical arbitrary waveform generation," *Nature Photon*., vol. 4, pp. 760–766, Oct. 2010.

[24] J. Zhang and J. P. Yao, "Time stretched sampling of a fast microwave waveform based on the repetitive use of a linearly chirped fiber Bragg grating in a dispersive loop," *Optica*, vol. 1, no. 2, pp. 64–69, Aug. 2014.

Jiejun Zhang (S'12) received the B.Eng. degree in electronic science and technology from Harbin Institute of Technology, Harbin, China, in 2010, and the M.Sc. degree in optical engineering from Huazhong University of Science and Technology, Wuhan, China. He is currently working toward the Ph.D. degree at the Microwave Photonics Research Laboratory, School of Electrical Engineering and Computer Science, University of Ottawa, Ottawa, ON, Canada.

His research interests include photonic generation of microwave waveforms, photonic processing of microwave signals, and fiber optic sensors.

Jianping Yao (M'99–SM'01–F'12) received the Ph.D. degree in electrical engineering from the Université de Toulon et du Var, Toulon, France, in December 1997.

He is a Professor and the University Research Chair in the School of Electrical Engineering and Computer Science, University of Ottawa, Ottawa, ON, Canada. From 1998 to 2001, he was with the School of Electrical and Electronic Engineering, Nanyang Technological University, Singapore, as an Assistant Professor. In December 2001, he joined the School of Electrical Engineering and Computer Science, University of Ottawa, as an Assistant Professor, where he was promoted to Associate Professor in 2003, and Full Professor in 2006. He was appointed as a University Research Chair in Microwave Photonics in 2007. In June 2016, he received the title of Distinguished University Professor of the University of Ottawa. From July 2007 to June 2010 and July 2013 to June 2016, he was the Director of the Ottawa-Carleton Institute for Electrical and Computer Engineering.

Dr. Yao has authored or co-authored more than 510 research papers, including more than 300 papers in peer-reviewed journals and 210 papers in conference proceedings. He is a Topical Editor for *Optics Letters*, and serves on the Editorial Boards of the IEEE TRANSACTIONS ON MICROWAVE THEORY AND TECHNIQUES, *Optics Communications*, *Frontiers of Optoelectronics*, and *Science Bulletin*. He was as a guest co-editor for a Focus Issue on Microwave Photonics in *Optics Express* in 2013 and a Lead-Editor for a Feature Issue on Microwave Photonics in *Photonics Research* in 2014. He is a Chair of numerous international conferences, symposia, and workshops, including the Vice Technical Program Committee (TPC) Chair of the IEEE Microwave Photonics Conference in 2007, TPC Co-Chair of the Asia-Pacific Microwave Photonics Conference in 2009 and 2010, TPC Chair of the high-speed and broadband wireless technologies subcommittee of the IEEE Radio Wireless Symposium in 2009-2012, TPC Chair of the microwave photonics subcommittee of the IEEE Photonics Society Annual Meeting in 2009, TPC Chair of the IEEE Microwave Photonics Conference in 2010, General Co-Chair of the IEEE Microwave Photonics Conference in 2011, TPC Co-Chair of the IEEE Microwave Photonics Conference in 2014, and General Co-Chair of the IEEE Microwave Photonics Conference in 2015. He is also a committee member of numerous international conferences, such as IPC, OFC, BGPP, and MWP. He received the 2005 International Creative Research Award of the University of Ottawa. He received the 2007 George S. Glinski Award for Excellence in Research. In 2008, he received a Natural Sciences and Engineering Research Council of Canada Discovery Accelerator Supplements Award. He was selected to receive an inaugural OSA Outstanding Reviewer Award in 2012. He was an IEEE MTT-S Distinguished Microwave Lecturer for 2013-2015.

He is a registered Professional Engineer of Ontario. He is a Fellow of the Optical Society of America, and the Canadian Academy of Engineering.